

Cite this: DOI: 10.1039/xxxxxxxxxx

Molecular electrometer and binding of cations to phospholipid bilayers[†]

Andrea Catte,^{a,‡} Mykhailo Giryh,^b Matti Javanainen,^{c,d} Claire Loison,^e Josef Melcr,^f Markus S. Miettinen,^{g,h} Luca Monticelli,ⁱ Jukka Määttä,^j Vasily S. Oganessian,^a O. H. Samuli Ollila,^{*b} Joona Tynkkynen,^c and Sergey Vilov,^e

Received Date
Accepted Date

DOI: 10.1039/xxxxxxxxxx

www.rsc.org/journalname

Despite the vast amount of experimental and theoretical studies on the binding affinity of cations into phospholipid bilayers, especially the biologically relevant Na⁺ and Ca²⁺ ions, there is no consensus in the literature. In this paper, we show that the ion binding affinity can be directly compared between simulations and experiments by using the choline headgroup order parameters according to the 'molecular electrometer' concept. Our findings strongly support the pre-2000 view that Na⁺ and other monovalent ions (except Li⁺) do not specifically bind to phosphatidylcholine lipid bilayers with mM concentrations, in contrast to Ca²⁺ and other multivalent ions. Especially the Na⁺ binding affinity is overestimated by several molecular dynamics simulation models, leading to an artificially positively charged lipid bilayer and overexaggerated structural effects in the headgroups. Qualitatively correct headgroup order parameter response is observed with Ca²⁺ binding in all the tested models, however, none of them has a sufficient quantitative accuracy to interpret the Ca²⁺:lipid stoichiometry or the induced atomistic resolution structural changes. This work has been done as a fully open collaboration, using nmrlipids.blogspot.fi as a main communication platform; all the scientific contributions were made publicly on this blog.

1 Introduction

Due to its high physiological importance — nerve cell signalling being the prime example — interaction of cations with phospholipid membranes has been widely studied via theory, simulations, and experiments. The relative ion binding affinities are generally agreed to follow the Hofmeister series^{1–9}, however, consensus

on the quantitative affinities is currently lacking. Until 1990, the consensus (documented in two extensive reviews^{2,3}) was that while multivalent cations interact significantly with phospholipid bilayers, for monovalent cations (with the exception of Li⁺) the interactions are weak. This conclusion has since been strengthened by further studies showing that bilayer properties remain unaltered upon the addition of sub-molar concentrations of monovalent salt^{4,10,11}. Since 2000, however, another view has emerged, suggesting much stronger interactions between phospholipids and monovalent cations, and strong Na⁺ binding in particular^{6–9,12–18}.

The pre-2000 view has the experimental support that (in contrast to the significant effects caused by any multivalent cations) sub-molar concentrations of NaCl have a negligible effect on phospholipid infrared spectra⁴, area per molecule¹⁰, dipole potential¹⁹, lateral diffusion¹¹, and choline head group order parameters²⁰; in addition, the water sorption isotherm of a NaCl–phospholipid system is highly similar to that of a pure NaCl solution — indicating that the ion–lipid interaction is very weak⁴.

The post-2000 'strong binding' view rests on experimental and above all simulational findings. At sub-molar NaCl concentrations, the rotational and translational dynamics of membrane-embedded fluorescent probes decrease^{7,9,12}, and Atomic Force Microscopy (AFM) experiments show changes in bilayer hard-

^a University of East Anglia, Norwich, United Kingdom

^b Department of Biomedical Engineering and Computational Science, Aalto University, Espoo, Finland

^c Tampere University of Technology, Tampere, Finland

^d University of Helsinki, Finland

^e Institut Lumière Matière, UMR5306 Université Lyon 1-CNRS, Université de Lyon, 69622 Villeurbanne, France

^f Institute of Organic Chemistry and Biochemistry, Czech Academy of Sciences, Flemingovo nám. 2, 16610 Prague 6, Czech Republic, Charles University in Prague, Faculty of Mathematics and Physics, Ke Karlovu 3, 121 16 Prague 2, Czech Republic

^g Fachbereich Physik, Freie Universität Berlin, Berlin, Germany

^h Max Planck Institute of Colloids and Interfaces, Department of Theory and Bio-Systems, Potsdam, Germany

ⁱ Institut de Biologie et Chimie des Protéines (IBCP), CNRS UMR 5086, Lyon, France

^j Aalto University, Espoo, Finland

* Author to whom correspondence may be addressed. E-mail: samuli.ollila@aalto.fi.

[†] Electronic Supplementary Information (ESI) available: 5 figures, detailed technical discussion and simulation details. See DOI: 10.1039/b000000x/

[‡] The authors are listed in alphabetical order.

ness^{14–18}; in atomistic molecular dynamics (MD) simulations, phospholipid bilayers consistently bind Na^+ , although the binding strength depends on the model used^{12,13,21–26}.

Some observables have been interpreted in favor of both views. For example, as the effect of monovalent ions (except Li^+) on the phase transition temperature is tiny (compared to the effect of multivalent ions), it was initially interpreted as an indication that only multivalent ions and Li^+ specifically bind to phospholipid bilayers²; however, such a small effect in calorimetric measurements was later interpreted to indicate that also Na^+ binds^{8,12}.

Similarly, the lack of significant positive electrophoretic mobility of phosphatidylcholine (PC) vesicles in the presence of NaCl (again in contrast to multivalent ions and Li^+) suggested weak binding of Na^+ ^{1,8,14,15,27}; however, these data have also been explained by a counteracting effect of the Cl^- ions^{22,28}.

Area per lipid was found to reduce in simulations upon Na^+ binding (e.g. Refs.^{12,23}) in agreement with AFM experiments^{14–18}; however, the reduction in area was observed at sub-molar Na^+ concentrations, whereas molar concentrations were required to reproduce the effect in scattering experiments¹⁰.

Lipid lateral diffusion was reported to be reduced in some simulation studies (e.g. Refs.¹²) upon Na^+ binding, supporting the interpretation of the reduced lateral diffusion of fluorescent probes^{7,9,12} as favoring the post-2000 view; however, reduction of lipid diffusion was not observed in noninvasive NMR experiments, suggesting that the fluorescence results arise from Na^+ interactions with probes rather than with lipids¹¹.

In the present paper we set out to solve the apparent contradictions between the pre-2000 and post-2000 views. To this end we employ the ‘molecular electrometer’ concept, according to which the changes in the order parameters of the α and β carbons in the phospholipid head group (see Fig. 1) can be used to measure the ion affinity to PC lipid bilayer^{20,29–31}. As order parameters can be accurately measured in experiments and directly compared to simulations³², employing the molecular electrometer as a function of cation concentration allows the comparison of binding affinity between simulations and experiments. In addition to demonstrating the usefulness of this general concept, we show that the response of order parameters to penetrating cations is qualitatively correct in MD simulations, but that in several models the affinity of Na^+ for PC bilayers is grossly overestimated. Moreover, we show that the accuracy of lipid- Ca^{2+} interactions in current models is not enough for atomistic resolution interpretation of NMR experiments.

This work has been done as an Open Collaboration at nmrlipids.blogspot.fi; all the related files (https://github.com/NMRLipids/lipid_ionINTERACTION) and almost all the simulation data (<https://zenodo.org/collection/user-nmrlipids>) are openly available.

2 Results and Discussion

2.1 Background: Molecular electrometer in experiments

The molecular electrometer concept is based on the experimental observation that binding of any charged objects on a PC bilayer interface induces systematic changes in the choline β and α

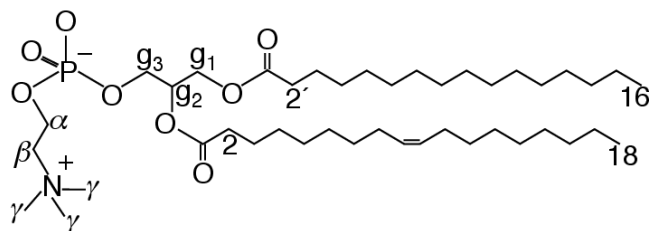


Fig. 1 Chemical structure of 1-palmitoyl-2-oleoylphosphatidylcholine (POPC), and the definition of γ , β , α , g_1 , g_2 and g_3 segments.

segment order parameters^{20,29–31,33–38}. Thus, these changes can be used to determine binding affinities of the charged objects. Molecular electrometer was originally devised for cations^{20,29}, but further experimental quantification with various positively and negatively charged molecules showed that the choline order parameters S_{CH}^{α} and S_{CH}^{β} in general vary linearly with small amount of bound charge per lipid^{29–31,33–38}. The empirically observed linear relation can be written as³⁹

$$S_{\text{CH}}^i(X^{\pm}) = S_{\text{CH}}^i(0) + \frac{4m_i}{3\chi} X^{\pm}, \quad (1)$$

where $S_{\text{CH}}^i(0)$ is the order parameter in the absence of bound charges, m_i empirical constant depending on the valency and position of bound charge, the quadrupole coupling constant $\chi \approx 167$ kHz, X^{\pm} is the amount of bound charge per lipid, and i refers to either α or β . The order parameter change with respect to a bilayer without bound charges then becomes

$$\Delta S_{\text{CH}}^i = S_{\text{CH}}^i(X^{\pm}) - S_{\text{CH}}^i(0) = \frac{4m_i}{3\chi} X^{\pm}. \quad (2)$$

For Ca^{2+} binding to POPC bilayer (in the presence of 100 mM NaCl), combination of atomic absorption spectra and ^2H NMR experiments gave $m_{\alpha} = -20.5$ and $m_{\beta} = -10.0$ ²⁹.

The absolute values of order parameters increase for β and decrease for α segment with bound positive charge and *vice versa* for negative charge^{20,29–31,33,38}. However, as the β carbon order parameter is negative while α carbon order parameter is positive^{40–42}, we can conclude that both $\Delta S_{\text{CH}}^{\beta}$ and $\Delta S_{\text{CH}}^{\alpha}$ decrease with bound positive charge and increase with bound negative charge. Consequently, values of m_i are negative for bound positive charges and *vice versa*. This can be rationalized by electrostatically induced changes in choline P-N dipole tilt^{30,31,44}, which is also seen in simulations^{23,24,45,46}. This is in line with order parameter decrease related to the P-N vector tilting more parallel to membrane plane seen with decreasing hydration levels⁴³.

The quantification of $\Delta S_{\text{CH}}^{\beta}$ and $\Delta S_{\text{CH}}^{\alpha}$ with different cations have revealed that $\Delta S_{\text{CH}}^{\beta} / \Delta S_{\text{CH}}^{\alpha} \approx 0.5$ for a wide range of differ-

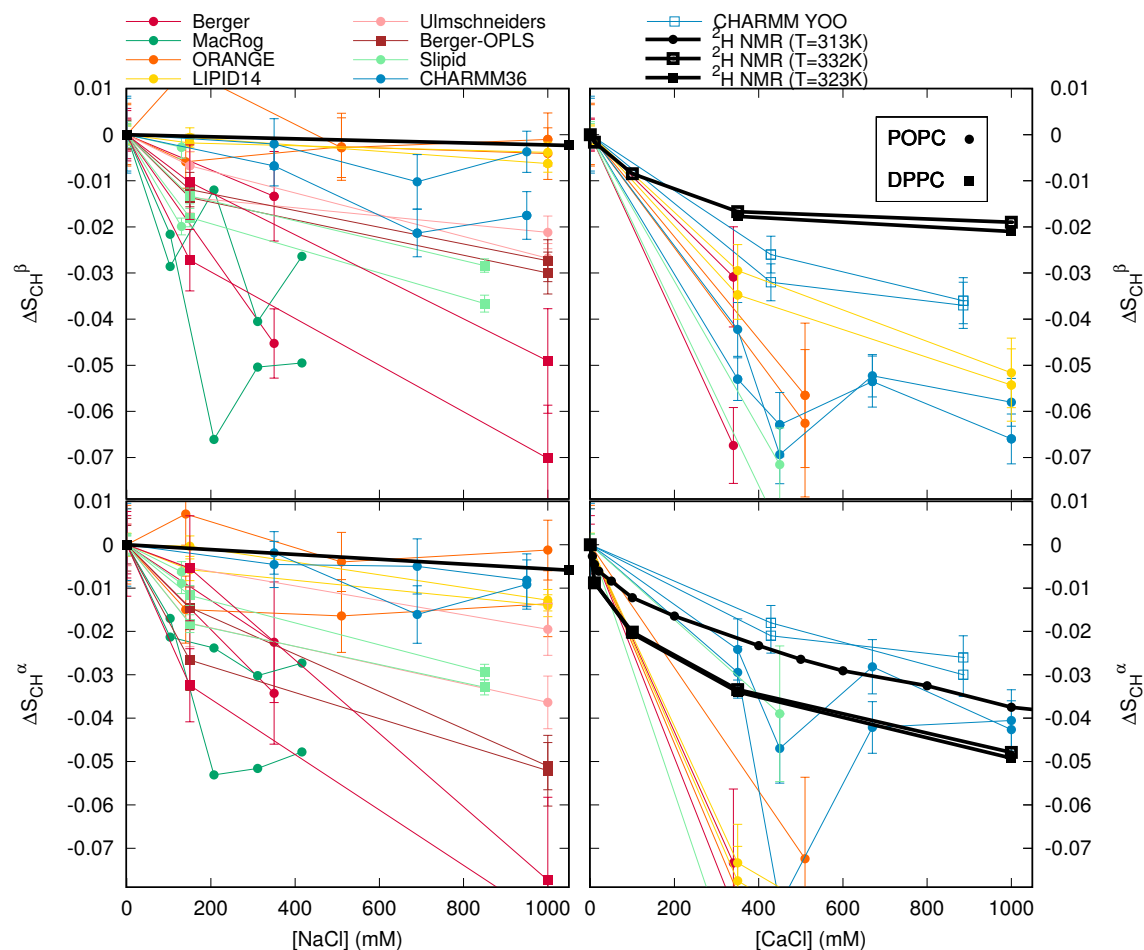


Fig. 2 The order parameter changes for β and α segments as a function of NaCl (left column) and CaCl_2 (right column) concentration, from simulations and experiments²⁰ (POPC with CaCl_2 from²⁹). The signs of the experimental order parameters, taken from experiments without ions^{40–42}, can be assumed to be unchanged with concentrations represented here^{29,32}. It should be noted that none of the models used here reproduces the order parameters within experimental error for pure PC bilayer without ions, indicating structural inaccuracies with varying severity in all models⁴³. Note that the relatively large decrease in CHARMM36 with 450 mM CaCl_2 arise from more equilibrated binding affinity due to long simulation times, see ESI[†].

ent cations (aqueous cations, cationic peptides, cationic anesthetics)^{36,38}. More specifically, the relation $\Delta S_{\text{CH}}^{\beta} = 0.43 \Delta S_{\text{CH}}^{\alpha}$ was found for a DPPC bilayer with various CaCl_2 concentrations²⁰.

2.2 Molecular electrometer concept in MD simulations

The headgroup order parameter changes as a function of ion concentration in solution from ^2H NMR experiments are shown in Fig. 2 for DPPC and POPC bilayers^{20,29}. Only minor changes in order parameters are seen as a function of NaCl in solution, while the effect of CaCl_2 is an order of magnitude larger. Thus, according to the molecular electrometer concept, monovalent Na^+ ions have negligible affinity for PC lipid bilayers at concentrations up to 1 M, while binding of Ca^{2+} ions at the same concentration is significant^{20,29}.

Figure 2 also reports order parameter changes calculated from MD simulations of DPPC and POPC lipid bilayers as a function of NaCl or CaCl_2 concentrations in solution (for details of the simulated systems see Tables 1, 2 and ESI[†]). Note that none of these MD models reproduced within experimental uncertainty the order parameters for a pure PC bilayer without ions (Figure 2 in

Ref. 43), indicating structural inaccuracies of varying severity in all models⁴³. However, the experimentally observed headgroup order parameter increase with dehydration was qualitatively reproduced by all the models⁴³, and similarly here the presence of cations leads to the decrease of S_{CH}^{β} and S_{CH}^{α} (Fig. 2), in qualitative agreement with experiments. The changes are, however, overestimated by most models. According to the electrometer concept this indicates overbinding of cations in most MD simulation models.

While electrometer concept is well established in experiments (see previous section), it is not *a priori* clear that it works in simulations. The overestimated order parameter decrease could, in principle, arise also from oversensitivity of choline headgroups on cation binding, instead of overbinding. Here we analyze the relation between cation binding and choline order parameter decrease in simulations in order to evaluate usability of electrometer concept in MD simulations.

According to the molecular electrometer concept, order parameter changes are linearly proportional to the amount of bound cations in bilayer (Eq. (2)). Figure 3 shows the order param-

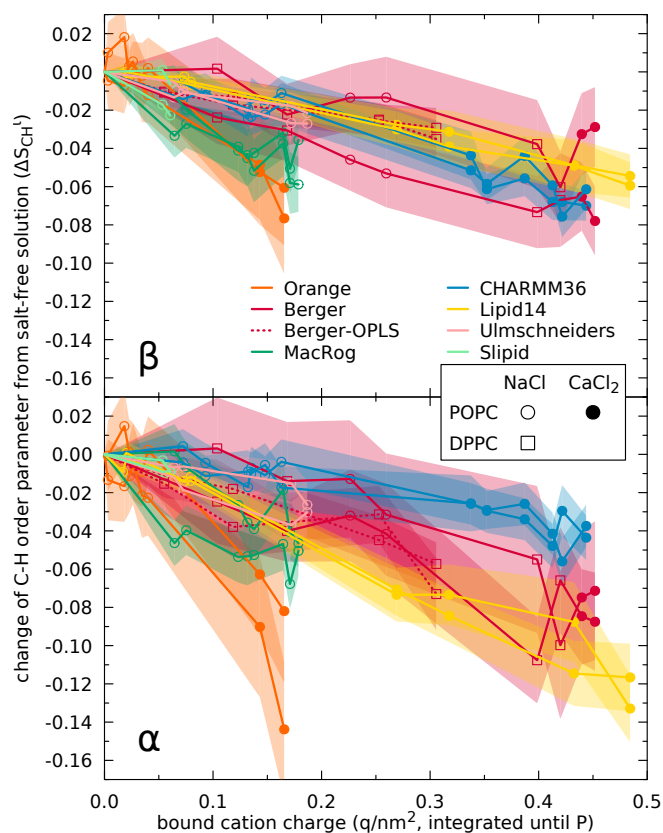


Fig. 3 Order parameters changes ΔS_{CH}^{β} and ΔS_{CH}^{α} as a function of bound cations from different simulation models.

1. Results from long CHARMM and Slipids simulations to be added. Description of the calculation of bound charges to be described, probably in supplementary.

ter changes as a function of bound charge in MD simulations; in keeping with the molecular electrometer, roughly linear correlation between bound charge and order parameter change is found in all models. Note that quantitative comparison of the proportionality constants (i.e. slopes in Fig. 3) between different models and experimental slopes ($m_{\alpha} = -20.5$ and $m_{\beta} = -10.0$ for Ca^{2+} binding in DPPC bilayer in the presence of 100mM NaCl in Eq. 1²⁹) is not straightforward since the simulation slopes depend on the definition used for bound ions.

The comparison of order parameter changes in response to bound charge is more straightforward for systems with charged amphiphiles fully associated in bilayer, as the amount of bound charge is then explicitly known in both simulations and experiments. Such comparison between previously published simulation data⁴⁷ and experiments^{31,48} could not rule out overestimation of order parameter response to bound cations (i.e., slopes m_{β} and m_{α}) in a Berger-based model (ESI[†]). This might, in principle, explain the overestimated order parameter response of Berger model to CaCl_2 , but not to NaCl (see discussion in ESI[†]). Since simulation data with charged amphiphiles from other models is not available, the extended comparison with different models is left for further studies.

Figure 3 shows that the order parameter decrease clearly correlates with the amount of bound cations also in simulations. This is

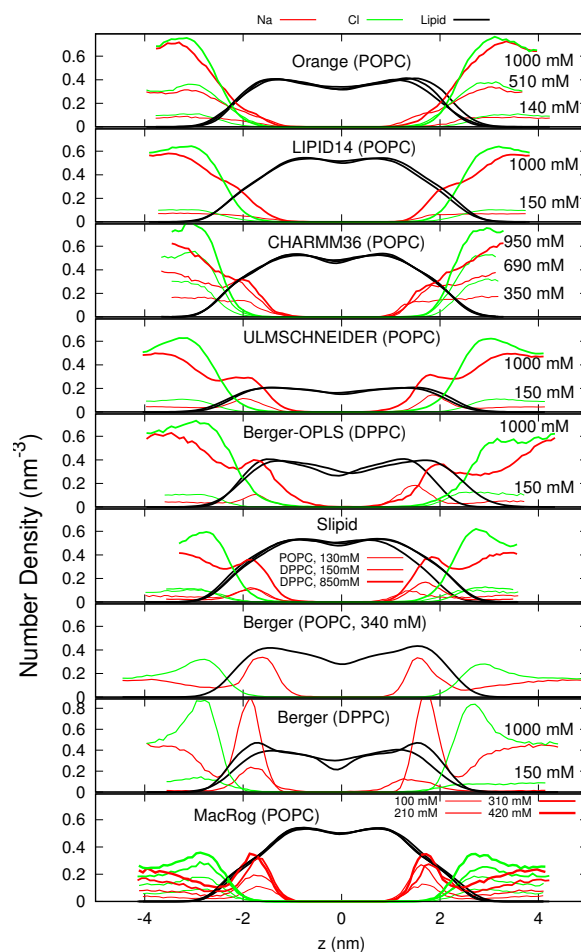


Fig. 4 Atom number density profiles along the membrane normal for lipids, Na^+ , and Cl^- ions from simulations with different force fields and different NaCl concentrations. The force fields are ordered according to the order parameter changes reported Fig. 2, from the smallest (top panel) to the largest (bottom panel). The lipid densities are scaled by 100 (united atom) or 200 (all atom model) to improve readability.

also evident from Fig. 4, which shows the Na^+ density profiles of the MD models ordered according to the order parameter change (reported in Fig. 2) from the smallest (top) to the largest (bottom). The Na^+ density peaks are larger for models with larger changes in order parameters, in line with the observed correlation between cation binding and order parameter decrease in Fig. 3.

Figure 5 compares the relation between ΔS_{CH}^{β} and ΔS_{CH}^{α} in experiments²⁰ and different simulation models. Only Lipid14 gives $\Delta S_{CH}^{\beta}/\Delta S_{CH}^{\alpha}$ ratio in agreement with the experimental ratio. In all the other models the α order parameter decrease with bound cations is underestimated in respect to β order parameter decrease.

In conclusion, the clear correlation between bound cations and order parameter decrease is observed in all the tested simulation models. Consequently, the electrometer concept can be used to compare the cation binding affinity between experiments and simulations. However, we find that the quantitative response of α and β segment order parameters to bound cations in simulations do not generally agree with the experiments. The $\Delta S_{CH}^{\beta}/\Delta S_{CH}^{\alpha}$ ra-

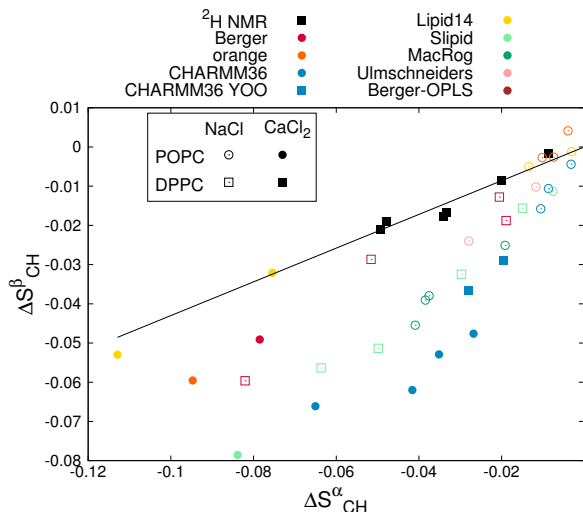


Fig. 5 Relation between $\Delta S_{\text{CH}}^{\beta}$ and $\Delta S_{\text{CH}}^{\alpha}$ from experiments²⁰ and different simulation models. Solid line is $\Delta S_{\text{CH}}^{\beta} = 0.43\Delta S_{\text{CH}}^{\alpha}$ determined for DPPC bilayer from ^2H NMR experiment with various CaCl_2 concentrations²⁰.

tio agrees with experiments only in Lipid14 model (Fig. 5). Thus, the observed overestimations of the order parameter changes with cation concentrations may, in principle, arise from overbinding of ions or from too sensitive lipid headgroup response on bound cation (see also discussion in ESI[†]). A careful analysis with current lipid models is performed in the next section.

2.3 Cation binding in different simulation models

The order parameter changes (Fig. 2) and density distributions (Fig. 4) demonstrate significantly different Na^+ binding affinities in different simulation models. The best agreement with experiments (lowest $\Delta S_{\text{CH}}^{\alpha}$ and $\Delta S_{\text{CH}}^{\beta}$) is observed for those models (Orange, CHARMM36, and Lipid14; see Fig. 2) that also predict the lowest Na^+ densities in the membrane proximity (Fig. 4). In all the other tested models, the choline order parameter responses to NaCl are clearly overestimated (Fig. 2), and the strength of the overestimation is clearly linked to the strength of the Na^+ binding affinity (compare Figs. 2 and 4); this leads us to conclude that sodium binding affinity is overestimated in all these models.

In the best three models, the order parameter changes with NaCl are small (< 0.02), so with the achieved statistical accuracy we cannot conclude which of the three has the most realistic Na^+ binding affinity, especially at physiological NaCl concentrations ($\sim 150\text{mM}$) relevant for most applications. The overestimated binding in the other models raise questions on the quality of the predictions from these models when NaCl is present. Especially interactions between charged molecules and lipid bilayer might be significantly affected by the strong Na^+ binding, as it makes the bilayer effectively positively charged.

Significant Ca^{2+} binding affinity to a phosphatidylcholine bilayer at mM concentrations is agreed in the literature^{2,3,20,29}, however, several details are yet under discussion. Simulations suggest that Ca^{2+} bind to lipid carbonyl oxygens with coordination number of 4.2¹³, while interpretation of NMR and scat-

tering experiments suggest that one Ca^{2+} interacts mainly with choline groups^{102–104} of two phospholipid molecules²⁹. Simulation model correctly reproducing the order parameter changes would resolve the discussion by giving atomistic resolution interpretation for the experiments.

As a function of CaCl_2 concentration, all but one (CHARMM36 with recent ion model by Yoo et al.⁷³), model overestimate the order parameter decrease (Fig. 2). According to the molecular electrometer, this indicates overestimated Ca^{2+} binding. This is the most likely scenario for the models where changes in both order parameters were overestimated, however, in the case of CaCl_2 we cannot exclude the possibility that the headgroup response is oversensitive to bound cations (see ESI[†]). In CHARMM36 with ion model by Yoo et al.⁷³, ΔS_{CH} is overestimated for β but underestimated for α , in line with Fig. 5 where $\Delta S_{\text{CH}}^{\beta}/\Delta S_{\text{CH}}^{\alpha}$ ratio in CHARMM36 is larger than in experiments. Since we do not know if $\Delta S_{\text{CH}}^{\beta}$ or $\Delta S_{\text{CH}}^{\alpha}$ is more realistic in CHARMM36, we cannot conclude if Ca^{2+} binding is too strong or weak in this simulation model. This could be resolved by comparing CHARMM36 model to the experimental data with known amount of bound charge (e.g., experiments with amphiphilic cations^{31,48}), however, such simulation data is not currently available.

The ion density distributions with CaCl_2 in Fig. 6 show significant Ca^{2+} binding in all models, however, some differences occur in details. The Berger model predicts deeper penetration depth (density maxima close to $\pm 1.8\text{ nm}$) compared to other models (density maxima close to $\pm 2\text{ nm}$). The latter value is probably more realistic since ^1H NMR and neutron scattering data indicate that Ca^{2+} interacts mainly with the choline group^{2,102–104}. In CHARMM36, almost all Ca^{2+} ions present in simulation bind in bilayer indicating strongest binding affinity among the tested models. The difference is not as clear in Fig. 2 because α carbon order parameters are least sensitive to bound charge in CHARMM36 (Fig. 3).

The origin of inaccuracies in lipid–ion interactions and binding affinities in different models is far from clear. Potential candidates could be, for example, discrepancies in the ion models^{105–107}, incomplete treatment of electronic polarizability¹⁰⁸, or inaccuracies in the lipid headgroup description⁴³. Cordomi et al.²⁴ showed that the Na^+ binding affinity decreases when ion radius increases in the model, however, also the models with the largest radius show significant binding in DPPC bilayer simulated with OPLS-AA force field¹⁰⁹. In our results, the Slipid model gives essentially similar binding affinity with ion parameters from Refs.⁸⁹ and^{84,85}. Further, the compensation of missing electronic polarizability by scaling ion charge^{108,110} reduced Na^+ binding in Berger, BergerOPLS and Slipid models, but not enough to be in agreement with experiments (ESI[†]). The charge-scaled Ca^{2+} model¹¹¹ slightly reduced binding in CHARMM36, but did not have significant influence on binding in Slipids (ESI[†]). Significant reduction of Ca^{2+} binding was observed with ion model by Yoo et al.⁷³, however, the CHARMM36 lipid model must be further analyzed to fully interpret the results.

On the other hand, also the lipid models may have significant influence on ion binding behaviour. For example, the same ion model and non-bonded parameters are used in the Orange and

Table 1 List of simulations performed in this work. The ion concentrations are calculated as $[\text{ion}] = (N_{\text{ion}} \times [\text{water}]) / N_w$, where $[\text{water}] = 55.5 \text{ M}$. These correspond the concentrations reported in the experiments by Akutsu et al.²⁰. The lipid force fields are named as in our previous work⁴³.

Force field (lipid, ion)	lipid	[Ion] mM	^a N _l	^b N _w	^c N _{Na}	^d N _{Ca}	^e N _{Cl}	^f T (K)	^g t _{sim} (ns)	^h t _{anal} (ns)	Files
Berger-POPC-07 ⁴⁹	POPC	0	128	7290	0	0	0	298	270	240	50
Berger-POPC-07 ⁴⁹ , ffgmx ⁵¹	POPC	340 (NaCl)	128	7202	44	0	44	298	110	50	52
Berger-POPC-07 ⁴⁹ , ffgmx ⁵¹	POPC	340 (CaCl ₂)	128	7157	0	44	88	298	108	58	53
Berger-DPPC-97 ⁵⁴	DPPC	0	72	2880	0	0	0	323	60	50	55
Berger-DPPC-97 ⁵⁴ , ffgmx ⁵¹	DPPC	150 (NaCl)	72	2880	8	0	8	323	120	60	56
Berger-DPPC-97 ⁵⁴ , ffgmx ⁵¹	DPPC	1000 (NaCl)	72	2778	51	0	51	323	120	60	57
BergerOPLS-DPPC-06 ⁵⁸	DPPC	0	72	2880	0	0	0	323	120	60	59
BergerOPLS-DPPC-06 ⁵⁸ , OPLS ⁶⁰	DPPC	150 (NaCl)	72	2880	8	0	8	323	120	60	61
BergerOPLS-DPPC-06 ⁵⁸ , OPLS ⁶⁰	DPPC	1000 (NaCl)	72	2778	51	0	51	323	120	60	62
CHARMM36 ⁶³	POPC	0	72	2242	0	0	0	303	30	20	64
CHARMM36 ⁶³ , CHARMM36 ⁶⁵	POPC	350 (NaCl)	72	2085	13	0	13	303	80	60	66
CHARMM36 ⁶³ , CHARMM36 ⁶⁵	POPC	690 (NaCl)	72	2085	26	0	26	303	73	60	67
CHARMM36 ⁶³ , CHARMM36 ⁶⁵	POPC	950 (NaCl)	72	2168	37	0	37	303	80	60	68
CHARMM36 ⁶³ , CHARMM36	POPC	350 (CaCl ₂)	128	6400	0	35	70	303	200	100	69
CHARMM36 ⁶³ , CHARMM36	POPC	450 (CaCl ₂)	200	9000	0	73	146	310	2000	100	70
CHARMM36 ⁶³ , CHARMM36	POPC	670 (CaCl ₂)	128	6400	0	67	134	303	200	120	71
CHARMM36 ⁶³ , CHARMM36	POPC	1000 (CaCl ₂)	128	6400	0	100	200	303	200	100	72
CHARMM36 ⁶³ , Yoo ⁷³	DPPC	430 (CaCl ₂)	128	7760	60	0	120	323	200	170	todo
CHARMM36 ⁶³ , Yoo ⁷³	DPPC	886 (CaCl ₂)	128	7520	120	0	240	323	200	170	todo
MacRog ⁷⁴	POPC	0	288	14400	0	0	0	310	90	40	75
MacRog ⁷⁴ , OPLS ⁶⁰	POPC	100 (NaCl)	288	14554	27	0	27	310	90	50	76
MacRog ⁷⁴ , OPLS ⁶⁰	POPC	210 (NaCl)	288	14500	54	0	54	310	90	50	76
MacRog ⁷⁴ , OPLS ⁶⁰	POPC	310 (NaCl)	288	14446	81	0	81	310	90	50	76
MacRog ⁷⁴ , OPLS ⁶⁰	POPC	420 (NaCl)	288	14392	108	0	108	310	90	50	76

^a The number of lipid molecules
^b The number of water molecules
^c The number of Na⁺ molecules
^d The number of Ca²⁺ molecules
^e The number of Cl molecules
^f Simulation temperature
^g The total simulation time
^h Time frames used in the analysis

Table 2 List of simulations performed in this work. The ion concentrations are calculated as $[\text{ion}] = (N_{\text{ion}} \times [\text{water}]) / N_w$, where $[\text{water}] = 55.5 \text{ M}$. These correspond to the concentrations reported in the experiments by Akutsu et al.²⁰. The lipid force fields are named as in our previous work⁴³.

Force field (lipid, ion)	lipid	[Ion] mM	cN_i	bN_w	cN_{Na}	eN_{Cl}	fT (K)	$g t_{\text{sim}}$ (ns)	$h t_{\text{anal}}$ (ns)	Files
Orange, OPLS ⁶⁰	POPC	0	72	2880	0	0	298	60	50	77
Orange, OPLS ⁶⁰	POPC	140 (NaCl)	72	2866	7	0	298	120	60	78
Orange, OPLS ⁶⁰	POPC	510 (NaCl)	72	2802	26	0	298	120	100	79
Orange, OPLS ⁶⁰	POPC	1000 (NaCl)	72	2780	50	0	298	120	80	80
Orange, OPLS	POPC	510 (CaCl ₂)	72	2802	0	26	298	120	60	81
Slipid ⁸²	DPPC	0	128	3840	0	0	323	150	100	83
Slipid ⁸² , AMBER ^{84,85}	DPPC	150 (NaCl)	600	18000	49	0	323	100	40	-
Slipid ⁸² , AMBER ^{84,85}	DPPC	850 (NaCl)	128	3726	57	0	323	105	100	86
Slipid ⁸⁷	POPC	0	128	5120	0	0	303	200	150	88
Slipid ⁸⁷ , AMBER ⁸⁹	POPC	130 (NaCl)	200	9000	21	0	310	105	100	90
Slipid ⁸⁷ , AMBER ⁶⁰	POPC	450 (CaCl)	200	9000	0	73	310	2000	100	91
Lipid14 ⁹² , AMBER ⁶⁰	POPC	0	128	5120	0	0	298	205	200	93
Lipid14 ⁹² , AMBER ⁶⁰	POPC	150 (NaCl)	128	5120	12	0	298	205	200	94
Lipid14 ⁹² , AMBER ⁶⁰	POPC	1000 (NaCl)	128	5120	77	0	298	205	200	95
Lipid14 ⁹² , AMBER ⁶⁰	POPC	350 (CaCl ₂)	128	6400	0	35	298	200	100	96
Lipid14 ⁹² , AMBER ⁶⁰	POPC	1000 (CaCl ₂)	128	6400	0	100	298	200	100	97
Ulmschneiders ⁹⁸ , OPLS ⁶⁰	POPC	0	128	5120	0	0	298.15	205	200	99
Ulmschneiders ⁹⁸ , OPLS ⁶⁰	POPC	150 (NaCl)	128	5120	12	0	298.15	205	200	100
Ulmschneiders ⁹⁸ , OPLS ⁶⁰	POPC	1000 (NaCl)	128	5120	77	0	298.15	205	200	101

a The number of lipid molecules

b The number of water molecules

c The number of Na⁺ molecules

d The number of Ca²⁺ molecules

e The number of Cl molecules

f Simulation temperature

g The total simulation time

h Time frames used in the analysis

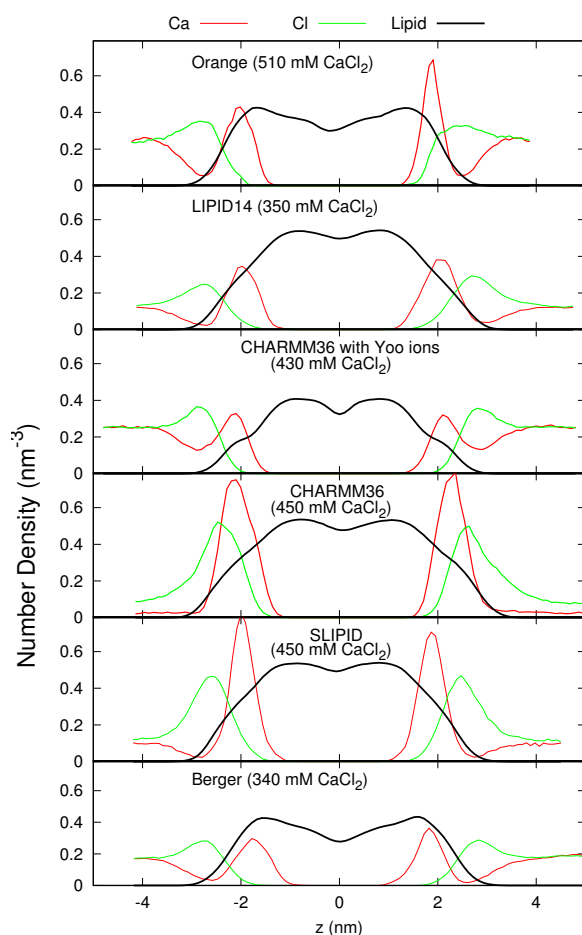


Fig. 6 Atom number density profiles along the membrane normal coordinate z for lipids, Ca^{2+} and Cl^- ions from simulations with different force fields. The profiles only with smallest available CaCl_2 concentration are shown for clarity. Figure including all the available concentrations is shown in ESI[†]. The lipid densities are scaled with 100 (united atom) or 200 (all atom model) to make them visible with the used y-axis scale. The Cl^- density is scaled with 2 to equalize charge density of ions.

BergerOPLS⁵⁸ simulations, but while Na^+ ion binding affinity appears realistic in the Orange model, it is significantly overestimated in the BergerOPLS (Fig. 4). However, realistic Na^+ binding does not directly relate to realistic Ca^{2+} binding (see Orange, Lipid14 and CHARMM36 in Fig. 2) or realistic choline order parameter response to bound charge (see Orange and CHARMM36 in Fig. 5). It should be also noted that the low binding affinity of Na^+ in CHARMM36 model is due to the additional repulsion added between sodium ions and lipid oxygens (NBFIX)⁶⁵ (ESI[†]). Altogether, our results indicate that probably both, lipid and ion force field parameters, need improvement to correctly predict the cation binding affinity, and the associated structural changes.

3 Conclusions

As suggested by the molecular electrometer concept^{20,29–31}, the decrease in order parameters of α and β carbons in the PC head group of lipids bilayers is related to cation binding in all tested simulation models (Fig. 3), despite of known inaccuracies in the actual atomistic resolution structures⁴³. Hence molecular elec-

trometer allows direct comparison of Na^+ binding affinity between simulations and noninvasive NMR experiments. The comparison reveals that most models overestimate Na^+ binding; only Orange, Lipid14, and CHARMM36 predict realistic binding affinity. None of the tested models has the required accuracy to interpret the Ca^{2+} :lipid stoichiometry or induced structural changes with atomistic resolution.

In general, our results support the pre-2000 view that at mM concentrations, in contrast to Ca^{2+} and other multivalent ions^{1–4,10,11,19,20,27,29}, Na^+ and other monovalent ions (except Li^+) do not specifically bind to phospholipid bilayers. Concerning the interpretation of existing experimental data, our work supports Cevc's view² that the observed small shift in phase transition temperature is not indicative of Na^+ binding. Further, our findings are in line with the noninvasive NMR spectroscopy work of Filippov et al.¹¹ that proved the results of Refs.^{7,9,12} to be explainable by direct interactions between Na^+ ions and fluorescent probes. Finally, as spectroscopic methods are in general more sensitive to atomistic details in fluid-like environment than AFM, our work indirectly suggests that the ion binding reported from AFM experiments on fluid-like lipid bilayer systems^{14–18} might be confounded with other physical features of the system. Concerning contradictions in MD simulation results, we reinterpret strong Na^+ binding as an artifact of several simulation models, e.g., the Berger model used in Refs.^{12,13}.

The artificial specific Na^+ binding in simulations may lead to doubtful results, since it effectively leads to positively charged phosphatidylcholine (PC) lipid bilayers even at physiological NaCl concentration. Such PC a bilayer has distinctly different interactions with charged objects compared to a (more realistic) model without specific Na^+ binding. Furthermore, the overestimation of Na^+ binding affinity may extend also to other positively charged objects, say, membrane protein segments. This would affect lipid–protein interactions and could explain, for example, contradicting results on electrostatic interactions between charged protein segments and lipid bilayer^{112,113}. In conclusion, more careful studies and model development on lipid bilayer–charged object interactions are called for to make molecular dynamics simulations directly usable in a physiologically relevant electrolytic environment.

This work has been done as a fully open collaboration, using nmrlipids.blogspot.fi as the communication platform. All the scientific contributions have been communicated publicly through this blog or GitHub repository https://github.com/NMRLipids/lipid_ionINTERACTION. All the related content and data is available at https://github.com/NMRLipids/lipid_ionINTERACTION.

Acknowledgements: OHSO acknowledges Tiago Ferreira for very useful discussions, the Emil Aaltonen foundation for financial support, Aalto Science-IT project and CSC-IT Center for Science for computational resources. MSM acknowledges financial support from the Volkswagen Foundation (86110). M.G. acknowledges financial support from Finnish Center of International Mobility (Fellowship TM-9363). J. M. acknowledges computational resources provided by the CESNET LM2015042 and the CERIT Scientific Cloud LM2015085 projects under the pro-

A Ion binding equilibration times

Simulations containing 450 mM CaCl_2 with CHARMM36 and Slipids were ran 2 μs to estimate the times required to equilibrate amount of bound Ca^{2+} in lipid bilayer. The amount of the bound calcium as a function of simulation time from these simulations are shown in Fig. 7. The results show clear increase in binding affinity up to 1000 ns and 700 ns in CHARMM36 and Slipids, respectively, and moderate increase even after this. This is also reflected to the CHARMM36 results in Fig. 2, where long CHARMM36 simulation with 450 mM CaCl_2 show relatively lower order parameters than shorter simulations. This can be rationalized with higher and more equilibrated binding affinity in long simulations. The results suggest that in other simulations the binding affinity is underestimated due to the insufficient equilibration times. This should be taken into account in more careful studies, but do not interfere the conclusion in this work that Ca^{2+} binding is most likely overestimated in all the other models than CHARMM36 with ion model by Yoo et al.⁷³.

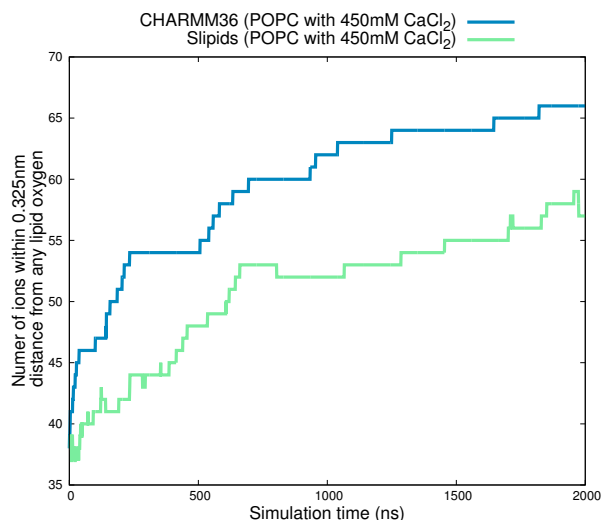


Fig. 7 Number of bound Ca^{2+} as a function of time from 2 μs long simulations with CHARMM36 and Slipids.

B Headgroup response on charged amphiphiles

The order parameter changes as a function of the bound charge cannot be straightforwardly compared between simulations and experiments from systems with ions because the results depend on the definition of bound ions in simulations. In systems with charged amphiphiles the situation is more straightforward since all the charges can be assumed to locate in bilayer in both, simulations and experiments. The order parameter changes as a function of charged amphiphiles, calculated from previously published simulation data^{47,114–116} and experiments^{31,48}, is shown in Fig 8.

The simulation data is from previously published binary mixture of cationic dimyristoyltrimethylammoniumpropane (DM-TAP) and zwitterionic (neutral) dimyristoylphosphatidylcholine

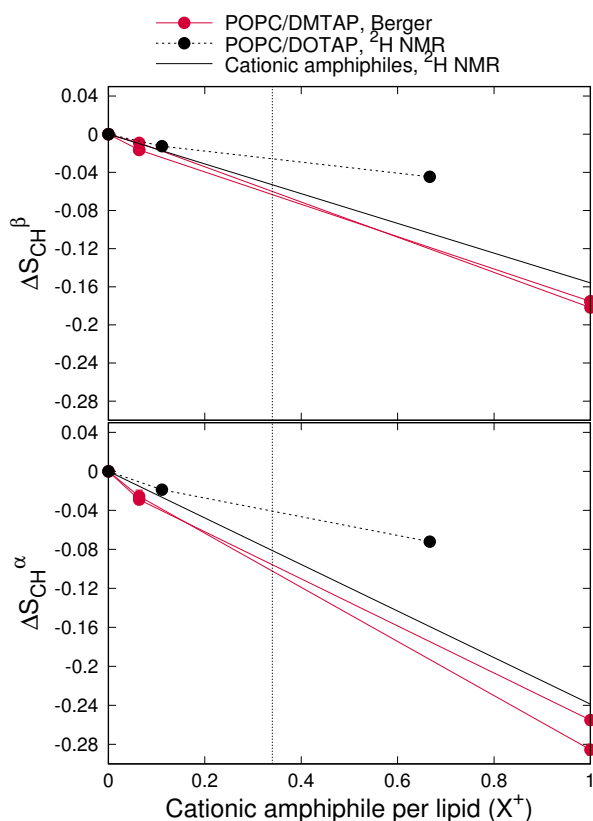


Fig. 8 Order parameter changes as a function of cationic amphiphiles from simulations^{47,114–116} and experiments^{31,48}. Experimental points for binary mixtures of POPC and 1,2-dioleoyloxy-3-(trimethylammonio)propane (DOTAP) are from⁴⁸. Experimental lines are from $\Delta S_{CH}^i = \frac{4}{3} \chi^{-1} m_i X^{\pm}$, where m_i are taken as average for different amphiphiles measured in 31.

(DMPC)^{47,114–116}, simulated with Berger based model. The experimental data from various amphiphiles with saturated acyl chains³¹ shown steeper slope than the data from DMPC/DOTAP mixtures⁴⁸. The origin of the difference is not known. It may arise, e.g., from the differences in acyl chain saturation level or headgroups of the amphiphiles. In the used simulation data the amphiphile acyl chains are fully saturated as in experimental data for various amphiphiles from 31, but the amphiphile headgroup and lipids are the same as in experimental data from 48. The order parameter changes from simulations overestimate the changes measured in latter experiment (especially with larger amphiphile concentrations), but are in good agreement with the former. However, the simulated system is not exactly the same as in experiments and also, the potential effect of Cl^- binding affinity cannot be excluded. Thus, with the available data we cannot accurately determine how realistic the headgroup response to bound charge is in simulation.

To estimate the maximum error we take the maximum amount of bound charge from Fig. 3 ($\approx 0.5 \frac{e}{\text{nm}^2}$) and assume the area per lipid of 0.68 nm^2 . This gives for maximum amount of bound charge per lipid $X_{\text{max}}^+ = 0.5 \frac{e}{\text{nm}^2} \cdot 0.68 \frac{\text{nm}^2}{\text{lipid}} = 0.34 \frac{e}{\text{lipid}}$, which is shown as dashed line in Fig. 8. The maximum overestimations of order parameter decrease with this amount of bound

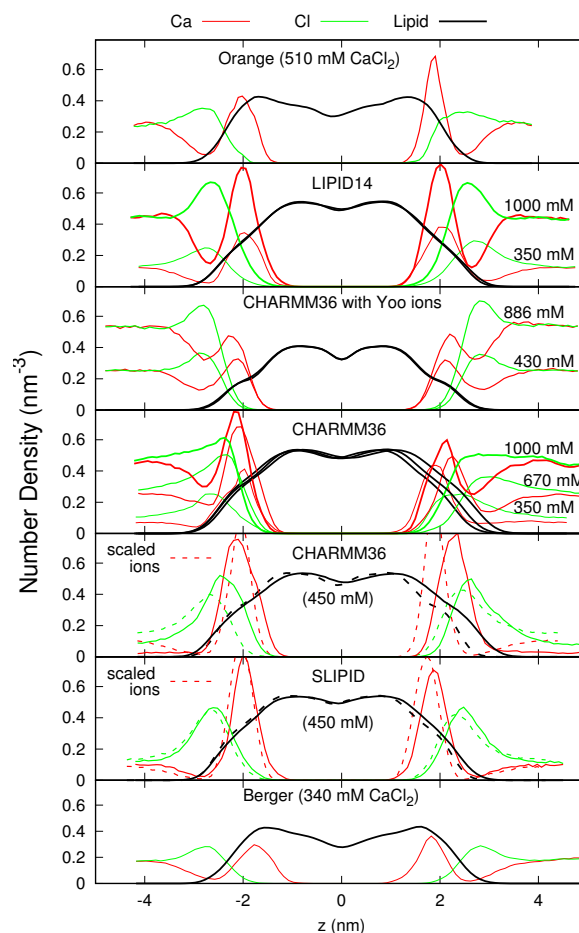


Fig. 9 Number density profiles for lipids, Ca^{2+} and Cl^- ions from simulations with different force fields and different CaCl_2 concentrations. The lipid densities are scaled with 100 (united atom) or 200 (all atom model) to make them visible with the used y-axis scale. The Cl^- density is scaled with 2 to equalize charge density of ions.

charge per lipid are ≈ 0.04 and ≈ 0.06 for β and α order parameter changes, respectively. The numbers are smaller with less amount of bound cations. In principle, these values could explain the overestimated order parameter change due to the presence of CaCl_2 in Berger model but not in the presence of NaCl (see Fig. 2).

In conclusion, with the current data we cannot fully exclude the possibility that the overestimated order parameter response to the CaCl_2 with Berger model arises from oversensitive headgroup response to bound cations. However, in the presence of NaCl the differences between responses in simulations and experiments in Fig. 2 are larger than the maximum estimated influence from a possible oversensitivity of the headgroup.

C Density distributions with different CaCl_2 concentrations

The density distributions with all simulated CaCl_2 concentrations are shown in Fig. 9.

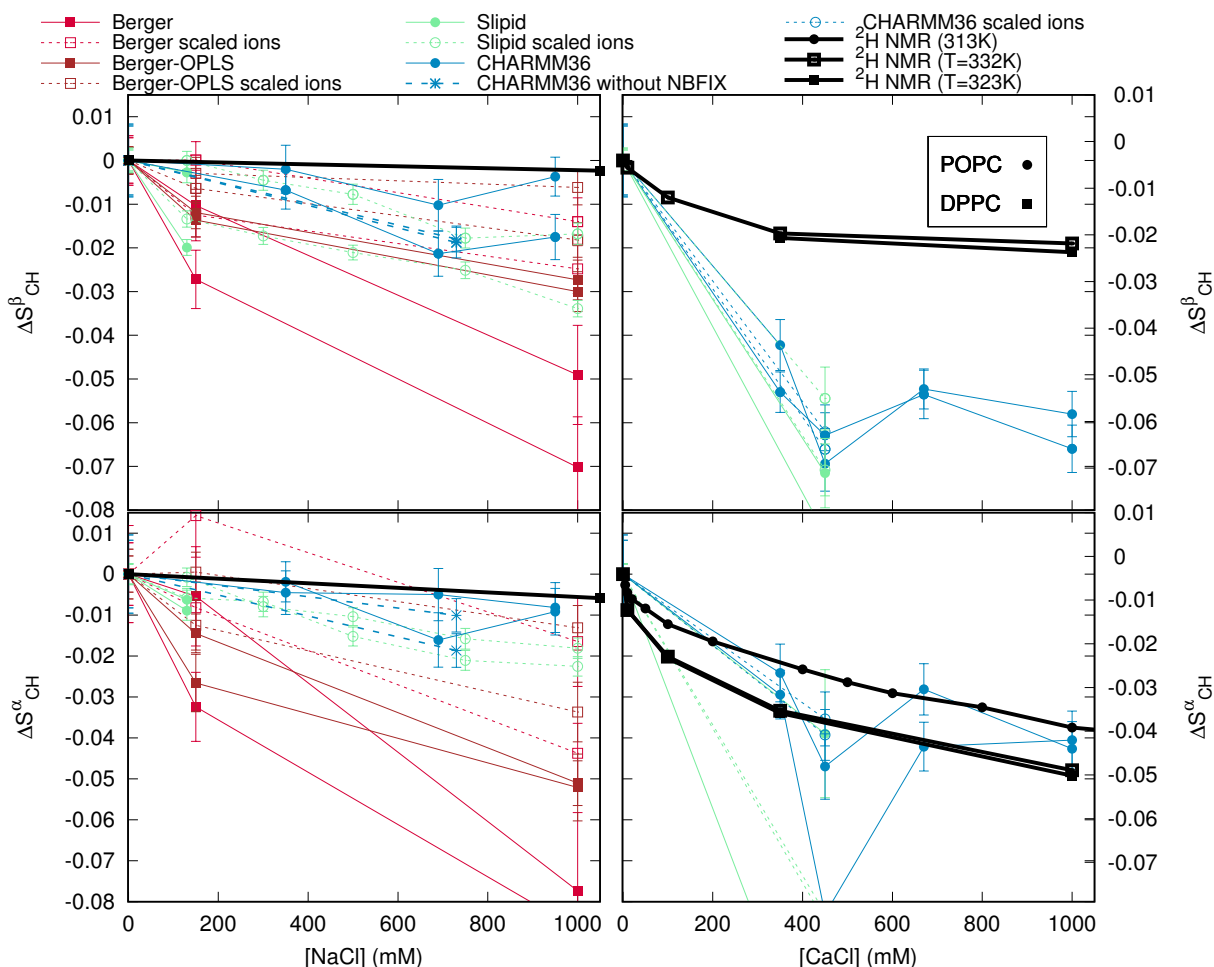


Fig. 10 The effect of charge scaling^{108,111} and NBFIX⁶⁵ on order parameter changes in simulations.

D Effect of ion model and polarization

It has been suggested that the missing electronic polarizability can be compensated by scaling the ion charge in simulations¹⁰⁸. To test if this would improve the Na^+ ion binding behaviour, we ran simulations with Berger-DPPC-97, BergerOPLS-DPPC-06 and Slipids with scaled Na^+ and Cl^- ions. For Berger-DPPC-97 and BergerOPLS-DPPC-06 models the ion charge in systems listed in Table 1 was simply scaled with 0.7 and the related files are available at ^{117–120}). For simulations with Slipids the ion model by Kohagen et al. was used¹¹⁰ and the related files are available at ¹²¹. The simulation parameters were identical to those employed in the simulation of POPC with 130 mM NaCl (see Methods). The order parameter changes and Na^+ -binding affinity are decreased by the charge scaling but yet overestimated with respect to the experiments as seen from Figs. 10 and 11. Thus the overestimated binding affinity cannot be fixed by only scaling the charges of ions.

The ion model for CaCl_2 with scaled charges¹¹¹ was tested with CHARMM36 and Slipid models. The related files are available at Refs. 122 and 123, respectively, and the results are shown in Figs. 9 and 10. The results with scaled charges are slightly improved but yet far from experiments.

Also the effect of NBFIX⁶⁵ on Na^+ binding in CHARMM36 is

quantified. The simulation data without NBFIX is available at¹²⁴. As expected, Figs. 10 and 11 show more significant order parameter decrease and higher Na^+ binding affinity without NBFIX. Thus, also the CHARMM36 model without NBFIX overestimates the Na^+ binding in PC bilayer.

E methods

E.1 Simulated systems

All simulations are ran with a standard setup for planar lipid bilayer in zero tension with periodic boundary conditions with Gromacs (version numbers 4.5-X-5.0.X)^{125,126} or NAMD¹²⁷ software packages.

E.2 Analysis

The order parameters were calculated from simulation trajectories directly applying the equation $S_{\text{CH}} = \langle \frac{3}{2} \cos^2 \theta - \frac{1}{2} \rangle$, where θ is the angle between a given C–H bond and the bilayer normal, and the average is taken over all lipids and time frames. For united atom models, the positions of hydrogen atoms were calculated for each molecule in each frame *a posteriori* by using the *g_protonate* tool in Gromacs 4.0.2¹²⁸. The statistical error in the order parameter was estimated by calculating the average value separately for each lipid molecule, and then the average and standard error of

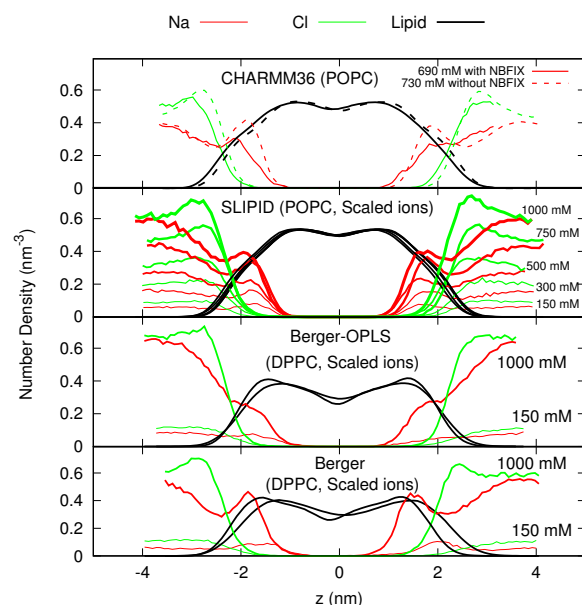


Fig. 11 Atom number density profiles along membrane normal coordinate z for lipids, Na^+ and Cl^- ions. The effect of NBFIX⁶⁵ on CHARMM36 simulation results is shown in top and other figures show the effect of ion models with scaled charges. The lipid densities are scaled with 100 (united atom) or 200 (all atom model) to make them visible with the used y-axis scale.

the mean over the ensemble of lipids (as done also in previous work⁴³). All the scripts used for analysis and the resulting data are available in the GitHub repository¹²⁹

E.3 Simulation details

E.3.1 Berger

POPC: The simulation without ions is the same as in Ref. 130 and the files are available at Ref. 50. The starting structures for simulations with ions is made by replacing water molecules with appropriate amount of ions (see Table 1). The Berger force field was used for the POPC¹³¹, with the dihedral potential next to the double bond taken from¹³². The ion parameters from ffgmx⁵¹ were used. Timestep of 2 fs was used with leap-frog integrator. Covalent bond lengths were constrained with LINCS algorithm^{133,134}. Coordinates were written every 10 ps. PME^{135,136} with real space cut-off at 1.0 nm was used for electrostatics. Plain cut-off was used for the Lennard-Jones interactions with a 1.0 nm cut-off. The neighbour list was updated every 5th step with cut-off at 1.0 nm. Temperature was coupled separately for lipids, water and ions to 298 K with the velocity-rescale method¹³⁷ with coupling constant 0.1 ps^{-1} . Pressure was semi-isotropically coupled to the atmospheric pressure with the Parrinello–Rahman barostat¹³⁸.

DPPC: The simulation without ions is the same as in⁴³ and the files are available at⁵⁵. The initial configuration contained 72 DPPC lipids and 2880 SPC water molecules. The standard Berger DPPC force field was used¹³¹ (simulations indicated as Berger-DPPC-97 in Table 1). The electrostatics were handled with PME^{135,136}, with real-space Coulomb cut-off set at 1.0 nm.

Lennard-Jones potentials were cut off at 1.0 nm. The neighbor list for all non-bonded interactions was updated every 10 steps. Temperature was set to 323K with the velocity-rescale method¹³⁷ using a coupling constant of 0.1 ps^{-1} . Semi-isotropic pressure coupling at 1 atm was handled with the Parrinello–Rahman barostat¹³⁸ with 1 ps coupling constant. The time step was 4 fs, and coordinates were written every 10 ps. The total simulation time was 120 ns (without pre-equilibration) and last 60 ns was used in the order parameter analysis.

For simulations with added salt, the appropriate number of SPC water molecules were randomly replaced with ions. Ions were described by the ffgmx parameters⁵¹. In simulations with scaled charges, charge-scaling was applied by scaling the ion charges by a factor 0.7. Conditions in the ion simulations were as with the pure DPPC described above. The duration of the simulations was 120 ns (without pre-equilibration) and last 60 ns was used in the order parameter analysis.

All the simulation files for pure DPPC simulations can be found at Ref. 55 and for the simulations with ions at Refs. 56,57 and with scaled ions at Refs. 117,118.

E.3.2 BergerOPLS

For simulations without ions, the initial configuration contains 72 DPPC lipids and 2880 SPC water molecules. For simulations with added salt, the appropriate amount of SPC water molecules were randomly replaced with ions. The number of ions is reported in Table 1. For the lipids, we used the same version of Berger force field as in previous simulations, described in¹³¹; for the ions, we used the Åqvist parameters⁶⁰ (commonly used within the OPLS-AA force field). Issues related to the compatibility between Berger and OPLS-AA force fields are described in ref.⁵⁸. A set of simulations was carried out using reduced electrostatic charges on the ions; in this case, a charge of 0.7 e was used on the ions, as described in refs.^{108,110}. Except for the ion force field, all simulation parameters (for non-bonded interactions, integration time step, thermostat, etc.) were identical to the parameters used in the Berger DPPC simulations described above.

All simulation files can be found at Ref. 59 for pure DPPC simulations, at Refs. 61,62 for simulations with ions, and at Refs. 119,120 for simulations with ions with scaled charges.

E.3.3 CHARMM36

POPC with NaCl: The simulation without ions is taken directly from Refs. 43,64. The starting structures for simulations with NaCl were made by replacing randomly located water molecules of the structure of pure POPC simulation with appropriate amount of ions. The force field for lipid were the same as in Refs. 43,64. The special TIP3P parameters for CHARMM36 and ion parameters with NBFIX by Venable et al.⁶⁵ were used. Simulations were ran with Gromacs 4.5.5 software¹²⁵. Timestep of 2 fs was used with leap-frog integrator. Covalent bonds with hydrogens were constrained with LINCS algorithm^{133,134}. Coordinates were written every 5 ps. PME with real space cut-off 1.4 nm was used for electrostatics. Lennard-Jones interactions were switched to zero between 0.8 nm and 1.2 nm. The neighbour list was updated every 5th step with cut-off 1.4 nm. Temperature was cou-

pled separately for lipids and solution to 303 K with the velocity-rescale method¹³⁷ with coupling constant 0.2 ps. Pressure was semi-isotropically coupled to the atmospheric pressure with the Berendsen method¹³⁹.

Simulation without NBFIX⁶⁵ was ran with the same settings, except that the temperature was kept at 310 K with Nosé–Hoover^{140,141} thermostat (simulation files available at Ref. 124).

POPC with CaCl_2 : The starting structures with varying amounts of CaCl_2 were constructed using the CHARMM-GUI Membrane Builder (<http://www.charmm-gui.org/>) online tool¹⁴². All runs were performed with Gromacs 5.0.3 software package¹²⁶ and CHARMM36 additive force field parameters for lipids⁶³ and ions were obtained from CHARMM-GUI input files. Simulation parameters provided by CHARMM-GUI were used. Particularly, the lengths of the bonds involving hydrogens were constrained with LINCS^{133,134}. The temperatures of the lipids and the solvent were separately coupled to the Nose–Hoover^{140,141} thermostat with a target temperature of 303 K and a relaxation time constant of 1.0 ps. Semi-isotropic pressure coupling to 1 bar was obtained with the Parrinello–Rahman barostat¹³⁸ with a time constant of 5 ps. Equations of motion were integrated with the Verlet algorithm¹⁴³ using a timestep of 2 fs. Long-range electrostatic interactions were calculated using the PME^{135,136} method with a fourth order smoothing spline. A real space cut-off of 1.2 nm was employed with grid spacing of 0.12 nm in the reciprocal space. Lennard-Jones interactions were smoothly switched to zero between 1.0 nm and 1.2 nm. Verlet cutoff-scheme¹⁴³ was used with the long-range neighbor list updated every 20 steps. Coordinates were written every 10 ps. After energy minimization and an equilibration run of 0.5 ns, 200 ns simulations were ran and the last 100 ns of each simulation was employed for the analysis.

DPPC with CaCl_2 (Yoo model): The systems contained 128 DPPC lipids and about 7600 TIP3P¹⁴⁴ water molecules, and an appropriate amount of ions as indicated in Table 1. We have used CHARMM36 additive force field parameters for lipids⁶³. In the calcium model developed recently by Yoo et al.⁷³, each cation is decorated by seven hydrating water molecules (with different charges from the usual TIP3P), which are constrained to remain in its vicinity. The associated parameter files are available on <http://bionano.physics.illinois.edu/CUFIX>. The constraint on the calcium-oxygen distances was imposed by adding extrabonds through a harmonic potential $V(r) = k(r - r_0)^2$, with $r_0 = 2.25 \text{ \AA}$ and $k = 10 \text{ kcal} \cdot \text{mol}^{-1} \cdot \text{\AA}^{-2}$.

The starting configuration of hydrated lipidic bilayers were constructed using *packmol*¹⁴⁵ with a large area per lipid (74 \AA^2). After a first energy minimization (5000 steps), varying amounts of Ca^{2+} and Cl^- ions were added by replacing water molecules, using the *autoionize* plugin of vmd package¹⁴⁶, mentioning explicitly the number of ions required. Ion placement is random, with the constraint of minimum 5 \AA between ions and lipids, as well as between any two ions. A second energy minimization was performed after inserting the ions.

All the minimizations and dynamics were conducted using the NAMD package¹²⁷. The temperature of the whole system was controlled with Langevin thermostat with a target temperature of 323 K and a relaxation time constant of 1 ps. The modified NAMD

version of Nose–Hoover barostat with Langevin dynamics (piston period of 0.1 ps and piston decay time of 0.05 ps) was used semi-isotropically for an average target pressure of 1 bar and an average zero surface tension. The equations of motion were integrated using the multiple time step Verlet r-RESPA algorithm¹⁴³ with a time step of 2 fs, and electrostatic forces calculated only every two time steps. Covalent bonds between heavy and hydrogen atoms were constrained using SHAKE/RATTLE algorithm. Long-range electrostatic interactions were calculated using the PME^{135,136} method with a 4-th order smoothing spline and a grid spacing of about 0.1 nm. A cut-off of 1.2 nm was employed for the Lennard-Jones interactions, with a force-based switching function for distances beyond 1 nm. Neighbor lists with a radius of 1.4 nm were updated every 10 timesteps. Coordinates were written every 20 ps. After energy minimization, a run of 200 ns simulations was performed, and the last ~ 170 ns of trajectory was employed for the analysis. Error bars are defined by \pm the standard error of the mean, taking into account the correlation time of the average order parameters (200 ps for 430 mM and 400 ps for 890 mM).

E.3.4 MacRog

The simulation parameters are identical to those employed in our earlier study⁴³ for the full hydration and dehydration simulations. The initial structures with varying amounts of NaCl were constructed from an extensively hydrated bilayer by replacing water molecules with ions using the Gromacs *genion* tool¹⁴⁷. Even at the highest considered salt concentration, the amount of water molecules per lipid after this replacement process was still greater than 50.

E.3.5 Orange

The systems contained 72 POPC lipids and 2880 SPC water molecules, and an appropriate amount of ions as indicated in Table 1.

For the lipids, we used an unpublished force field coined Orange force field. Briefly, this includes most bonded interactions from Berger lipids¹³¹, except for dihedrals which were derived via *ab initio* calculations on small model compounds. As in Berger lipids, Lennard-Jones parameters are from OPLS^{148–152}. Partial charges were derived on the basis of *ab initio* calculations. In simulations with ions, the Åqvist parameters were used⁶⁰. The electrostatics were handled with PME^{135,136}, with real-space Coulomb cut-off set at 1.8 nm. Lennard-Jones potentials were cut off at 1.8 nm. The neighbor lists for the calculation of non-bonded forces were updated every 5 steps.

Temperature was set to 298K with the velocity-rescale thermostat¹³⁷ using a coupling constant of 0.1 ps^{-1} , and the pressure was set to 1 bar using the Berendsen weak coupling algorithm¹³⁹ (compressibility of $4.5 \cdot 10^{-5} \text{ bar}^{-1}$, time constant of 1 ps), coupling separately the x-y dimension and the z dimension to obtain a tensionless system. A time step of 2 fs was used for the integration (with the leap-frog algorithm), coordinates were written every 100 ps, and the total simulation time was 60 ns.

Simulation files for pure lipid simulations are found at Ref. 77 and for the simulations with ions at Refs. 78–81.

E.3.6 Slipids

DPPE: The simulation without ions from Ref. 43, available at Ref. 83, was used. For the simulation with 150 mM NaCl, the starting DPPE lipid bilayer, which was built with the online CHARMM-GUI¹⁴² (<http://www.charmm-gui.org/>), contained 600 lipids hydrated by 30 water molecules per lipid.

For the simulation with 850 mM NaCl, the configuration from Ref. 83 was taken and an appropriate amount of water molecules was converted to ions to form a neutral NaCl solution. The simulation files are available at Ref. 86. Ion parameters by Roux^{84,85}, TIP3P water model¹⁴⁴ and Stockholm lipids (Slipids) parameters^{82,87} for phospholipids were used. GROMACS software package version 4.5.5 or 5.0.7¹²⁵ was employed for all simulations. After energy minimization and a short equilibration run of 50 ps (time step 1 fs), 100 ns production runs were performed using a time step of 2 fs with leap-frog integrator. All covalent bonds were constrained with the LINCS^{133,134} algorithm. Coordinates were written every 100 ps. PME^{135,136} with real space cut-off at 1.0 nm was used for Coulomb interactions. Lennard-Jones interactions were switched to zero between 1.0 nm and 1.4 nm. The neighbour lists were updated every 10th step with a cut-off of 1.6 nm. Temperature was coupled separately for upper and bottom leaflets of the lipid bilayer, and for water to 323 K with the Nosé-Hoover thermostat^{140,141} using a time constant of 0.5 ps. Pressure was semi-isotropically coupled to the atmospheric pressure with the Parrinello-Rahman¹³⁸ barostat using a time constant of 10 ps.

POPC: The simulation without ions from Ref. 43, available at Ref. 88 was used.

POPC with NaCl: A POPC bilayer consisting of 200 lipids, hydrated with 45 water molecules per lipid, was simulated in the presence of 130 mM NaCl. The Slipids model^{82,87} was employed for lipids, the TIP3P model¹⁴⁴ for water, and the ion parameters by Smith and Dang⁸⁹ for NaCl. The system was first equilibrated for 5 ns with a time step of 1 fs after which a 100 ns production run was performed using a time step of 2 fs. Trajectories were written every 100 ps. The system was kept in a tensionless state at 1 bar using a semi-isotropic Parrinello–Rahman barostat¹³⁸ with a time constant of 1 ps. The temperature was maintained at 310 K with the velocity rescaling thermostat¹³⁷. The time constant was set to 0.5 ps for both lipids and solvent (water and ions) which were coupled separately. Non-bonded interactions were calculated within a neighbor list with a radius of 1 nm and an update interval of 10 steps. The Lennard-Jones interactions were cut-off at 1 nm, whereas PME^{135,136} was employed for long-range electrostatics. Dispersion correction was applied to both energy and pressure. All bonds were constrained with the LINCS^{133,134} algorithm.

POPC with CaCl₂: A POPC bilayer consisting of 200 lipids, hydrated with 45 water molecules per lipid, was simulated in the presence of 450 mM CaCl₂. The system was ran for 2000 ns and the last 100 ns was used for analysis. Other details are as in POPC with NaCl.

E.3.7 Lipid14

The starting structures with varying amounts of ions were constructed using the CHARMM-GUI Membrane Builder (<http://www.charmm-gui.org/>) online tool¹⁴². The GROMACS compatible force field parameters generated in Ref. 43 and available at Ref. 153 were used. The TIP3P water model¹⁴⁴ was used to solvate the system and Åqvist⁶⁰ parameters were used for ions. All runs were performed with Gromacs 5.0.3 software package¹²⁶ and LIPID14 force field parameters for POPC⁹².

H-bond lengths were constrained with LINCS^{133,134}. The temperatures of the lipids and the solvent were separately coupled to the Nose–Hoover^{140,141} thermostat with a target temperature of 298.15 K and a relaxation time constant of 0.1 ps. Semi-isotropic pressure coupling to 1 bar was obtained with the Parrinello-Rahman barostat¹³⁸ with a time constant of 2 ps. Equations of motion were integrated with the Verlet algorithm¹⁴³ using a timestep of 2 fs. Long-range electrostatic interactions were calculated using the PME^{135,136} method with a fourth order smoothing spline. A real space cut-off at 1.0 nm was employed with grid spacing of 0.12 nm in the reciprocal space. Lennard-Jones potentials were cut-off at 1 nm, with a dispersion correction applied to both energy and pressure. Verlet cutoff-scheme¹⁴³ were used with the long-range neighbor list updated every 20 steps. Coordinates were written every 10 ps.

After energy minimization and an equilibration run of 5 ns, 200 ns production runs were performed and analysed. In case of the CaCl₂ systems only the last 100 ns of each simulation was employed for the analysis.

E.3.8 Ulmschneiders

The starting structures with varying amounts of ions were constructed using the CHARMM-GUI Membrane Builder (<http://www.charmm-gui.org/>) online tool¹⁴². The force field parameters were obtained from Lipidbook¹⁵⁴. The TIP3P water model¹⁴⁴ was used to solvate the system. Additionally, the simulations of ion-free bilayer were repeated with both Verlet and Group cutoff-schemes⁹⁹. There was no significant difference in headgroup or glycerol backbone order parameters between these cutoff-schemes. All runs were performed with Gromacs 5.0.3 software package¹²⁶. The glycerol backbone order parameters without ions were not the same as reported in the previous study⁴³. The origin of discrepancy was located to the different initial structures which was taken from CHARMM-GUI in this work and from Lipidbook in the previous work. Since the order parameters with the initial structure from CHARMM-GUI are closer to the experimental values, the results indicate that the structure available from Lipidbook is stuck to a state with incorrect glycerol backbone structure, for more discussion see https://github.com/NMRLipids/lipid_ionINTERACTION/issues/8.

All-bond lengths were constrained with LINCS^{133,134}. The temperatures of the lipids and the solvent were separately coupled to the Nose–Hoover^{140,141} thermostat with a target temperature of 298.15 K and a relaxation time constant of 0.1 ps. Semi-isotropic pressure coupling to 1 bar was obtained with the Parrinello-Rahman barostat¹³⁸ with a time constant of 2 ps. Equations of motion were integrated with the Verlet algorithm¹⁴³ using a

timestep of 2 fs. Long-range electrostatic interactions were calculated using the PME^{135,136} method with a fourth order smoothing spline. A real space cut-off at 1.0 nm was employed with grid spacing of 0.12 nm in the reciprocal space. Lennard-Jones potentials were cut-off at 1 nm, with a dispersion correction applied to both energy and pressure. Verlet cutoff-scheme¹⁴³ were used with the long-range neighbor list updated every 20 steps. Coordinates were written every 10 ps. After energy minimization and an equilibration run of 5 ns, 200 ns simulations were ran and the last 100 ns of each simulation was employed for the analysis.

F Author Contributions

Andrea Catte

Mykhailo Grych ran and analyzed several simulations. Discussed the project actively with OHSO.

Matti Javanainen provided data with several lipid and ion models. Discussed the project actively with OHSO. Supervised the work of JT.

Claire Loison provided results for CHARMM36 DPPC+CaCl₂ with Yoo's model.

Josef Melcr performed and analyzed several simulations; discussed the project actively; corrected and contributed to the manuscript.

Markus S. Miettinen

Luca Monticelli

Jukka Määttä

Vasily S. Oganessian

O. H. Samuli Ollila co-designed the project with MSM and managed the work. Ran and analyzed several simulations. Wrote the manuscript.

Joona Tynkkynen

Sergey Vilov provided results for CHARMM36 DPPC+CaCl₂ with Yoo's model.

ToDo

1. Results from long CHARMM and Slipids simulations to be added. Description of the calculation of bound charges to be described, probably in supplementary. 4

References

- 1 M. Eisenberg, T. Gresalfi, T. Riccio and S. McLaughlin, *Biochemistry*, 1979, **18**, 5213–5223.
- 2 G. Cevc, *Biochim. Biophys. Acta - Rev. Biomemb.*, 1990, **1031**, 311 – 382.
- 3 J.-F. Tocanne and J. Teissié, *Biochim. Biophys. Acta - Reviews on Biomembranes*, 1990, **1031**, 111 – 142.
- 4 H. Binder and O. Zschörnig, *Chem. Phys. Lipids*, 2002, **115**, 39 – 61.
- 5 J. J. Garcia-Celma, L. Hatahet, W. Kunz and K. Fendler, *Langmuir*, 2007, **23**, 10074–10080.
- 6 E. Leontidis and A. Aroti, *J. Phys. Chem. B*, 2009, **113**, 1460–1467.
- 7 R. Vacha, S. W. I. Siu, M. Petrov, R. A. Böckmann, J. Baruch-Kraszewska, P. Jurkiewicz, M. Hof, M. L. Berkowitz and P. Jungwirth, *J. Phys. Chem. A*, 2009, **113**, 7235–7243.
- 8 B. Klasczyk, V. Knecht, R. Lipowsky and R. Dimova, *Langmuir*, 2010, **26**, 18951–18958.
- 9 F. F. Harb and B. Tinland, *Langmuir*, 2013, **29**, 5540–5546.
- 10 G. Pabst, A. Hodzic, J. Strancar, S. Danner, M. Rappolt and P. Laggner, *Biophys. J.*, 2007, **93**, 2688 – 2696.
- 11 A. Filippov, G. Orädd and G. Lindblom, *Chem. Phys. Lipids*, 2009, **159**, 81 – 87.
- 12 R. A. Böckmann, A. Hac, T. Heimburg and H. Grubmüller, *Biophys. J.*, 2003, **85**, 1647 – 1655.
- 13 R. A. Böckmann and H. Grubmüller, *Ang. Chem. Int. Ed.*, 2004, **43**, 1021–1024.
- 14 S. Garcia-Manyes, G. Oncins and F. Sanz, *Biophys. J.*, 2005, **89**, 1812 – 1826.
- 15 S. Garcia-Manyes, G. Oncins and F. Sanz, *Electrochim. Acta*, 2006, **51**, 5029 – 5036.
- 16 T. Fukuma, M. J. Higgins and S. P. Jarvis, *Phys. Rev. Lett.*, 2007, **98**, 106101.
- 17 U. Ferber, G. Kaggwa and S. Jarvis, *Eur. Biophys. J.*, 2011, **40**, 329–338.
- 18 L. Redondo-Morata, G. Oncins and F. Sanz, *Biophys. J.*, 2012, **102**, 66 – 74.
- 19 R. J. Clarke and C. Lüpfer, *Biophys. J.*, 1999, **76**, 2614 – 2624.
- 20 H. Akutsu and J. Seelig, *Biochemistry*, 1981, **20**, 7366–7373.
- 21 J. N. Sachs, H. Nanda, H. I. Petrache and T. B. Woolf, *Biophys. J.*, 2004, **86**, 3772 – 3782.
- 22 M. L. Berkowitz, D. L. Bostick and S. Pandit, *Chem. Rev.*, 2006, **106**, 1527–1539.
- 23 A. Cordoní, O. Edholm and J. J. Perez, *J. Phys. Chem. B*, 2008, **112**, 1397–1408.
- 24 A. Cordoní, O. Edholm and J. J. Perez, *J. Chem. Theory Comput.*, 2009, **5**, 2125–2134.
- 25 C. Valley, J. Perlmutter, A. Braun and J. Sachs, *J. Membr. Biol.*, 2011, **244**, 35–42.
- 26 M. L. Berkowitz and R. Vacha, *Acc. Chem. Res.*, 2012, **45**, 74–82.
- 27 S. A. Tatulian, *Eur. J. Biochem.*, 1987, **170**, 413–420.
- 28 V. Knecht and B. Klasczyk, *Biophys. J.*, 2013, **104**, 818 – 824.
- 29 C. Altenbach and J. Seelig, *Biochemistry*, 1984, **23**, 3913–3920.
- 30 J. Seelig, P. M. MacDonald and P. G. Scherer, *Biochemistry*, 1987, **26**, 7535–7541.
- 31 P. G. Scherer and J. Seelig, *Biochemistry*, 1989, **28**, 7720–7728.
- 32 O. S. Ollila and G. Pabst, *Atomistic resolution structure and dynamics of lipid bilayers in simulations and experiments*, 2016, <http://dx.doi.org/10.1016/j.bbamem.2016.01.019>, In Press.
- 33 C. Altenbach and J. Seelig, *Biochim. Biophys. Acta*, 1985, **818**, 410 – 415.
- 34 P. M. Macdonald and J. Seelig, *Biochemistry*, 1987, **26**,

- 1231–1240.
- 35 M. Roux and M. Bloom, *Biochemistry*, 1990, **29**, 7077–7089.
 - 36 G. Beschiaschvili and J. Seelig, *Biochim. Biophys. Acta - Biomembranes*, 1991, **1061**, 78 – 84.
 - 37 F. M. Marassi and P. M. Macdonald, *Biochemistry*, 1992, **31**, 10031–10036.
 - 38 J. R. Rydall and P. M. Macdonald, *Biochemistry*, 1992, **31**, 1092–1099.
 - 39 T. M. Ferreira, R. Sood, R. Bärenwald, G. Carlström, D. Topgaard, K. Saalwächter, P. K. Kinnunen and S. O. Ollila, *Acyl chain disorder and azelaoyl orientation in lipid membranes containing oxidized lipids*, 0, <http://dx.doi.org/10.1021/acs.langmuir.6b00788>, PMID: 27260273.
 - 40 M. Hong, K. Schmidt-Rohr and A. Pines, *J. Am. Chem. Soc.*, 1995, **117**, 3310–3311.
 - 41 M. Hong, K. Schmidt-Rohr and D. Nanz, *Biophys. J.*, 1995, **69**, 1939 – 1950.
 - 42 J. D. Gross, D. E. Warschawski and R. G. Griffin, *J. Am. Chem. Soc.*, 1997, **119**, 796–802.
 - 43 A. Botan, F. Favela-Rosales, P. F. J. Fuchs, M. Javanainen, M. Kanduć, W. Kulig, A. Lamberg, C. Loison, A. Lyubartsev, M. S. Miettinen, L. Monticelli, J. Määttä, O. H. S. Ollila, M. Retegan, T. Róg, H. Santuz and J. Tynkkynen, *J. Phys. Chem. B*, 2015, **119**, 15075–15088.
 - 44 J. Seelig, *Cell Biol. Int. Rep.*, 1990, **14**, 353–360.
 - 45 A. A. Gurtovenko, M. Miettinen, M. Karttunen and I. Vattulainen, *J. Phys. Chem. B*, 2005, **109**, 21126–21134.
 - 46 W. Zhao, A. A. Gurtovenko, I. Vattulainen and M. Karttunen, *J. Phys. Chem. B*, 2012, **116**, 269–276.
 - 47 M. S. Miettinen, A. A. Gurtovenko, I. Vattulainen and M. Karttunen, *J. Phys. Chem. B*, 2009, **113**, 9226–9234.
 - 48 C. M. Franzin, P. M. Macdonald, A. Polozova and F. M. Winnik, *Biochim. Biophys. Acta - Biomembranes*, 1998, **1415**, 219 – 234.
 - 49 S. Ollila, M. T. Hyvönen and I. Vattulainen, *J. Phys. Chem. B*, 2007, **111**, 3139–3150.
 - 50 O. H. S. Ollila, T. Ferreira and D. Topgaard, *MD simulation trajectory and related files for POPC bilayer (Berger model delivered by Tieleman, Gromacs 4.5)*, 2014, <http://dx.doi.org/10.5281/zenodo.13279>.
 - 51 T. P. Straatsma and H. J. C. Berendsen, *J. Chem. Phys.*, 1988, **89**, year.
 - 52 O. H. S. Ollila, *MD simulation trajectory and related files for POPC bilayer with 340mM NaCl (Berger model delivered by Tieleman, ffgmx ions, Gromacs 4.5)*, 2015, <http://dx.doi.org/10.5281/zenodo.32144>.
 - 53 O. H. S. Ollila, *MD simulation trajectory and related files for POPC bilayer with 340mM CaCl₂ (Berger model delivered by Tieleman, ffgmx ions, Gromacs 4.5)*, 2015, <http://dx.doi.org/10.5281/zenodo.32173>.
 - 54 S.-J. Marrink, O. Berger, P. Tieleman and F. Jähnig, *Biophys. J.*, 1998, **74**, 931 – 943.
 - 55 J. Määttä, *DPPC_Berger*, 2015, <http://dx.doi.org/10.5281/zenodo.13934>.
 - 56 J. Määttä, *DPPC_Berger_NaCl*, 2015, <http://dx.doi.org/10.5281/zenodo.16319>.
 - 57 J. Määttä, *DPPC_Berger_NaCl_1Mol*, 2015, <http://dx.doi.org/10.5281/zenodo.17210>.
 - 58 D. P. Tieleman, J. L. MacCallum, W. L. Ash, C. Kandt, Z. Xu and L. Monticelli, *J. Phys. Condens. Matter*, 2006, **18**, S1221.
 - 59 J. Määttä, *DPPC_Berger_OPLS06*, 2015, <http://dx.doi.org/10.5281/zenodo.17237>.
 - 60 J. Åqvist, *J. Phys. Chem.*, 1990, **94**, 8021–8024.
 - 61 J. Määttä, *DPPC_Berger_OPLS06_NaCl*, 2015, <http://dx.doi.org/10.5281/zenodo.16484>.
 - 62 J. Määttä, *DPPC_Berger_OPLS06_NaCl_1Mol*, 2016, <http://dx.doi.org/10.5281/zenodo.46152>.
 - 63 J. B. Klauda, R. M. Venable, J. A. Freites, J. W. O'Connor, D. J. Tobias, C. Mondragon-Ramirez, I. Vorobyov, A. D. M. Jr and R. W. Pastor, *J. Phys. Chem. B*, 2010, **114**, 7830–7843.
 - 64 O. H. S. Ollila and M. Miettinen, *MD simulation trajectory and related files for POPC bilayer (CHARMM36, Gromacs 4.5)*, 2015, <http://dx.doi.org/10.5281/zenodo.13944>.
 - 65 R. M. Venable, Y. Luo, K. Gawrisch, B. Roux and R. W. Pastor, *J. Phys. Chem. B*, 2013, **117**, 10183–10192.
 - 66 O. H. S. Ollila, *MD simulation trajectory and related files for POPC bilayer with 350mM NaCl (CHARMM36, Gromacs 4.5)*, 2015, <http://dx.doi.org/10.5281/zenodo.32496>.
 - 67 O. H. S. Ollila, *MD simulation trajectory and related files for POPC bilayer with 690mM NaCl (CHARMM36, Gromacs 4.5)*, 2015, <http://dx.doi.org/10.5281/zenodo.32497>.
 - 68 O. H. S. Ollila, *MD simulation trajectory and related files for POPC bilayer with 950mM NaCl (CHARMM36, Gromacs 4.5)*, 2015, <http://dx.doi.org/10.5281/zenodo.32498>.
 - 69 M. Girych and O. H. S. Ollila, *POPC_CHARMM36_CaCl₂_035Mol*, 2015, <http://dx.doi.org/10.5281/zenodo.35159>.
 - 70 M. Javanainen, *POPC @ 310K, 450 mM of CaCl₂. Charmm36 with default Charmm ions*, 2016, <http://dx.doi.org/10.5281/zenodo.51185>.
 - 71 M. Girych and O. H. S. Ollila, *POPC_CHARMM36_CaCl₂_067Mol*, 2015, <http://dx.doi.org/10.5281/zenodo.35160>.
 - 72 M. Girych and O. H. S. Ollila, *POPC_CHARMM36_CaCl₂_1Mol*, 2015, <http://dx.doi.org/10.5281/zenodo.35156>.
 - 73 J. Yoo, J. Wilson and A. Aksimentiev, *Biopolymers*, 2016.
 - 74 A. Maciejewski, M. Pasenkiewicz-Gierula, O. Cramariuc, I. Vattulainen and T. Rog, *J. Phys. Chem. B*, 2014, **118**, 4571–4581.
 - 75 M. Javanainen, 2014.
 - 76 M. Javanainen, *POPC @ 310K, varying amounts of NaCl. Model by Maciejewski and Rog*, 2015, <http://dx.doi.org/10.5281/zenodo.14976>.
 - 77 O. H. S. Ollila, J. Määttä and L. Monticelli, *MD simulation trajectory for POPC bilayer (Orange, Gromacs 4.5.)*, 2015, <http://dx.doi.org/10.5281/zenodo.34488>.

- 78 O. H. S. Ollila, J. Määttä and L. Monticelli, *MD simulation trajectory for POPC bilayer with 140mM NaCl (Orange, Gromacs 4.5.)*, 2015, <http://dx.doi.org/10.5281/zenodo.34491>.
- 79 O. H. S. Ollila, J. Määttä and L. Monticelli, *MD simulation trajectory for POPC bilayer with 510mM NaCl (Orange, Gromacs 4.5.)*, 2015, <http://dx.doi.org/10.5281/zenodo.34490>.
- 80 S. Ollila, J. Määttä and L. Monticelli, *MD simulation trajectory for POPC bilayer with 1000mM NaCl (Orange, Gromacs 4.5.)*, 2015, <http://dx.doi.org/10.5281/zenodo.34497>.
- 81 O. H. S. Ollila, J. Määttä and L. Monticelli, *MD simulation trajectory for POPC bilayer with 510mM CaCl₂ (Orange, Gromacs 4.5.)*, 2015, <http://dx.doi.org/10.5281/zenodo.34498>.
- 82 J. P. M. Jämbeck and A. P. Lyubartsev, *J. Phys. Chem. B*, 2012, **116**, 3164–3179.
- 83 J. Määttä, *DPPC_Slipids*, 2014, <http://dx.doi.org/10.5281/zenodo.13287>.
- 84 D. Beglov and B. Roux, *J. Chem. Phys.*, 1994, **100**, 9050–9063.
- 85 B. Roux, *Biophys. J.*, 1996, **71**, 3177 – 3185.
- 86 J. Melcr, *Simulation files for DPPC lipid membrane with Slipids force field for Gromacs MD simulation engine*, 2016, <http://dx.doi.org/10.5281/zenodo.55322>.
- 87 J. P. M. Jämbeck and A. P. Lyubartsev, *J. Chem. Theory Comput.*, 2012, **8**, 2938–2948.
- 88 M. Javanainen, *POPC @ 310K, Slipids force field.*, 2015, DOI: 10.5281/zenodo.13887.
- 89 D. E. Smith and L. X. Dang, *J. Chem. Phys.*, 1994, **100**, year.
- 90 M. Javanainen, *POPC @ 310K, 130 mM of NaCl. Slipids with ions by Smith & Dang*, 2015, <http://dx.doi.org/10.5281/zenodo.35275>.
- 91 M. Javanainen, *POPC @ 310K, 450 mM of CaCl₂. Slipids with default Amber ions*, 2016, <http://dx.doi.org/10.5281/zenodo.51182>.
- 92 C. J. Dickson, B. D. Madej, Å. A. Skjevik, R. M. Betz, K. Teigen, I. R. Gould and R. C. Walker, *J. Chem. Theory Comput.*, 2014, **10**, 865–879.
- 93 M. Girych and O. H. S. Ollila, *POPC_AMBER_LIPID14_Verlet*, 2015, <http://dx.doi.org/10.5281/zenodo.30898>.
- 94 M. Girych and O. H. S. Ollila, *POPC_AMBER_LIPID14_NaCl_015Mol*, 2015, <http://dx.doi.org/10.5281/zenodo.30891>.
- 95 M. Girych and O. H. S. Ollila, *POPC_AMBER_LIPID14_NaCl_1Mol*, 2015, <http://dx.doi.org/10.5281/zenodo.30865>.
- 96 M. Girych and O. H. S. Ollila, *POPC_AMBER_LIPID14_CaCl₂_035Mol*, 2015, <http://dx.doi.org/10.5281/zenodo.34415>.
- 97 M. Girych and O. H. S. Ollila, *POPC_AMBER_LIPID14_CaCl₂_1Mol*, 2015, <http://dx.doi.org/10.5281/zenodo.35074>.
- 98 J. P. Ulmschneider and M. B. Ulmschneider, *J. Chem. Theory Comput.*, 2009, **5**, 1803–1813.
- 99 M. Girych and O. H. S. Ollila, *POPC_Ulmschneider_OPLS_Verlet_Group*, 2015, <http://dx.doi.org/10.5281/zenodo.30904>.
- 100 M. Girych and O. H. S. Ollila, *POPC_Ulmschneider_OPLS_NaCl_015Mol*, 2015, <http://dx.doi.org/10.5281/zenodo.30892>.
- 101 M. Girych and O. H. S. Ollila, *POPC_Ulmschneider_OPLS_NaCl_1Mol*, 2015, <http://dx.doi.org/10.5281/zenodo.30894>.
- 102 H. Hauser, M. C. Phillips, B. Levine and R. Williams, *Nature*, 1976, **261**, 390 – 394.
- 103 H. Hauser, W. Guyer, B. Levine, P. Skrabal and R. Williams, *Biochim. Biophys. Acta - Biomembranes*, 1978, **508**, 450 – 463.
- 104 L. Herbert, C. Napolitano and R. McDaniel, *Biophys. J.*, 1984, **46**, 677 – 685.
- 105 B. Hess, C. Holm and N. van der Vegt, *J. Chem. Phys.*, 2006, **124**, year.
- 106 A. A. Chen, and R. V. Pappu, *J. Phys. Chem. B*, 2007, **111**, 11884–11887.
- 107 M. M. Reif, M. Winger and C. Oostenbrink, *J. Chem. Theory Comput.*, 2013, **9**, 1247–1264.
- 108 I. Leontyev and A. Stuchebrukhov, *Phys. Chem. Chem. Phys.*, 2011, **13**, 2613–2626.
- 109 W. L. Jorgensen, D. S. Maxwell and J. Tirado-Rives, *J. Am. Chem. Soc.*, 1996, **118**, 11225–11236.
- 110 M. Kohagen, P. E. Mason and P. Jungwirth, *J. Phys. Chem. B*, 2016, **120**, 1454–1460.
- 111 M. Kohagen, P. E. Mason and P. Jungwirth, *J. Phys. Chem. B*, 2014, **118**, 7902–7909.
- 112 A. Arkhipov, Y. Shan, R. Das, N. Endres, M. Eastwood, D. Wemmer, J. Kuriyan and D. Shaw, *Cell*, 2013, **152**, 557 – 569.
- 113 K. Kaszuba, M. Grzybek, A. Orłowski, R. Danne, T. Róg, K. Simons, Å. Coskun and I. Vattulainen, *Proc. Natl. Acad. Sci. USA*, 2015, **112**, 4334–4339.
- 114 M. S. Miettinen, *Molecular dynamics simulation trajectory of a fully hydrated DMPC lipid bilayer*, 2013, <http://dx.doi.org/10.5281/zenodo.51635>.
- 115 M. S. Miettinen, *Molecular dynamics simulation trajectory of a cationic lipid bilayer: 6/94 mol% DMTAP/DMPC*, 2016, <http://dx.doi.org/10.5281/zenodo.51639>.
- 116 M. S. Miettinen, *Molecular dynamics simulation trajectory of a cationic lipid bilayer: 50/50 mol% DMTAP/DMPC*, 2016, <http://dx.doi.org/10.5281/zenodo.51748>.
- 117 J. Määttä, *DPPC_Berger_NaCl_scaled*, 2015, <http://dx.doi.org/10.5281/zenodo.16320>.
- 118 J. Määttä, *DPPC_Berger_NaCl_1Mol_scaled*, 2015, <http://dx.doi.org/10.5281/zenodo.17228>.
- 119 J. Määttä, *DPPC_Berger_OPLS06_NaCl_scaled*, 2015, <http://dx.doi.org/10.5281/zenodo.16485>.
- 120 J. Määttä, *DPPC_Berger_OPLS06_NaCl_1Mol_scaled*, 2015,

- <http://dx.doi.org/10.5281/zenodo.17209>.
- 121 M. Javanainen, *POPC @ 310K, varying amounts of NaCl. Slipids with ECC-scaled ions*, 2015, <http://dx.doi.org/10.5281/zenodo.35193>.
- 122 M. Javanainen, *POPC @ 310K, 450 mM of CaCl₂. Charmm36 with ECC-scaled ions*, 2016, <http://dx.doi.org/10.5281/zenodo.45008>.
- 123 M. Javanainen, *POPC @ 310K, 450 mM of CaCl₂. Slipids with ECC-scaled ions*, 2016, <http://dx.doi.org/10.5281/zenodo.45007>.
- 124 J. Melcr, *Simulation files for POPC lipid membrane with Charmm36 force field without NBFIX for Gromacs MD simulation engine*, 2016, <http://dx.doi.org/10.5281/zenodo.55318>.
- 125 S. Pronk, S. Páll, R. Schulz, P. Larsson, P. Bjelkmar, R. Apostolov, M. R. Shirts, J. C. Smith, P. M. Kasson, D. van der Spoel, B. Hess and E. Lindahl, *Bioinformatics*, 2013, **29**, 845–854.
- 126 M. J. Abraham, T. Murtola, R. Schulz, S. Páll, J. C. Smith, B. Hess and E. Lindahl, *SoftwareX*, 2015, **1-2**, 19–25.
- 127 J. C. Phillips, R. Braun, W. Wang, J. Gumbart, E. Tajkhorshid, E. Villa, C. Chipot, R. D. Skeel, L. Kalé and K. Schulten, *J. Comput. Chem.*, 2005, **26**, 1781–1802.
- 128 D. van der Spoel, E. Lindahl, B. Hess, A. R. van Buuren, E. Apol, P. J. Meulenhoff, D. P. Tieleman, A. L. T. M. Sijbers, K. A. Feenstra, R. van Drunen and H. J. C. Berendsen, *GROMACS user manual version 4.0*, 2005.
- 129 O. H. S. Ollila and et al., 2015, https://github.com/NMRLipids/lipid_ionINTERACTION.
- 130 T. M. Ferreira, F. Coreta-Gomes, O. H. S. Ollila, M. J. Moreno, W. L. C. Vaz and D. Topgaard, *Phys. Chem. Chem. Phys.*, 2013, **15**, 1976–1989.
- 131 O. Berger, O. Edholm and F. Jähnig, *Biophys. J.*, 1997, **72**, 2002 – 2013.
- 132 M. Bachar, P. Brunelle, D. P. Tieleman and A. Rauk, *J. Phys. Chem. B*, 2004, **108**, 7170–7179.
- 133 B. Hess, H. Bekker, H. J. C. Berendsen and J. G. E. M. Fraaije, *J. Comput. Chem.*, 1997, **18**, 1463–1472.
- 134 B. Hess, *J. Chem. Theory Comput.*, 2008, **4**, 116–122.
- 135 T. Darden, D. York and L. Pedersen, *J. Chem. Phys.*, 1993, **98**, year.
- 136 U. L. Essman, M. L. Perera, M. L. Berkowitz, T. Larden, H. Lee and L. G. Pedersen, *J. Chem. Phys.*, 1995, **103**, 8577–8592.
- 137 G. Bussi, D. Donadio and M. Parrinello, *J. Chem. Phys.*, 2007, **126**, year.
- 138 M. Parrinello and A. Rahman, *J. Appl. Phys.*, 1981, **52**, 7182–7190.
- 139 H. J. C. Berendsen, J. P. M. Postma, W. F. van Gunsteren, A. DiNola and J. R. Haak, *J. Chem. Phys.*, 1984, **81**, 3684–3690.
- 140 S. Nose, *Mol. Phys.*, 1984, **52**, 255–268.
- 141 W. G. Hoover, *Phys. Rev. A*, 1985, **31**, 1695–1697.
- 142 J. Lee, X. Cheng, J. M. Swails, M. S. Yeom, P. K. Eastman, J. A. Lemkul, S. Wei, J. Buckner, J. C. Jeong, Y. Qi, S. Jo, V. S. Pande, D. A. Case, I. Charles L. Brooks, J. Alexander D. Mackerell, J. B. Klauda and W. Im, *J. Chem. Theory Comput.*, 2016, **12**, 405–413.
- 143 S. Páll and B. Hess, *Computer Physics Communications*, 2013, **184**, 2641 – 2650.
- 144 W. L. Jorgensen, J. Chandrasekhar, J. D. Madura, R. W. Impey and M. L. Klein, *J. Chem. Phys.*, 1983, **79**, year.
- 145 L. Martínez, R. Andrade, E. G. Birgin and J. M. Martínez, *J. Comput. Chem.*, 2009, **30**, 2157–2164.
- 146 W. Humphrey, A. Dalke and K. Schulten, *J. Mol. Graphics*, 1996, **14**, 33–38.
- 147 M. Abraham, D. van der Spoel, E. Lindahl, B. Hess and the GROMACS development team, *GROMACS user manual version 5.0.7*, 2015.
- 148 W. L. Jorgensen, J. D. Madura and C. J. Swenson, *J. Am. Chem. Soc.*, 1984, **106**, 6638–6646.
- 149 W. L. Jorgensen and J. Gao, *J. Phys. Chem.*, 1986, **90**, 2174–2182.
- 150 W. L. Jorgensen, *J. Phys. Chem.*, 1986, **90**, 1276–1284.
- 151 W. L. Jorgensen and J. Tirado-Rives, *J. Am. Chem. Soc.*, 1988, **110**, 1657–1666.
- 152 J. M. Briggs, T. B. Nguyen and W. L. Jorgensen, *J. Phys. Chem.*, 1991, **95**, 3315–3322.
- 153 O. H. S. Ollila and M. Retegan, *MD simulation trajectory and related files for POPC bilayer (Lipid14, Gromacs 4.5)*, 2014, <http://dx.doi.org/10.5281/zenodo.12767>.
- 154 J. Domański, P. Stansfeld, M. Sansom and O. Beckstein, *J. Membr. Biol.*, 2010, **236**, 255–258.